図7 小腸用カプセル内視鏡(PillCam™SB，左)と食道用カプセル内視鏡(PillCam™ESO，右)

図8 大腸用カプセル内視鏡(PillCam™COLON)

より開発された[6]．PillCam™ESOは，食道静脈瘤，GERD（gastroesophageal reflux disease)やバレット食道などを適応として，2004年にヨーロッパとアメリカのFDAに認可され，近い将来日本にも導入されるであろう．

さらに，最近新たに開発された大腸用カプセル内視鏡PillCam™COLONの外観を図8に示す．大きさは31×11 mmとPillCam™SBやPillCam™ESOの26×11 mmより大きいが，両方向の透明ドームは360度の画像撮影が可能で撮影範囲が格段に広がっている．両方向それぞれで1秒4枚の写真を撮影するが，カプセル作動開始後，食道と胃を約5分間撮影したのち2時間休止モードになり，その後再び撮影を開始するように設計されている．前処置を行って透明な液の中をカプセルが進むため，大腸のヒダの裏側でも非常に鮮明な画像が撮影される．大腸内視鏡検査との前向き比較試験[7,8]が行われた結果，2006年10月にヨーロッパで認可され，アメリカでも近々認可される見込みである．

これらカプセル内視鏡の技術は急速に進歩している．小腸だけでなく食道や大腸においてもスクリーニングが目的の場合は，将来的には現在用いられている軟性鏡に代わってカプセル内視鏡が主役になる可能性が高い．

おわりに

カプセル内視鏡は，筒型の硬性鏡あるいはチューブ型の軟性鏡など従来の内視鏡と全く異なるコンセプトで開発された．患者の苦痛なしに，生理的な状態の消化管内腔を診断することができる非侵襲的な検査法であり，高齢者にとって大きな福音といえよう．日本では，小腸用カプセル内視鏡であるPillCam™SBが薬事承認されたばかりであるが，海外では食道用(PillCam™ESO)や大腸用(PillCam™COLON)が実用化され，すでに臨床応用されている．IT技術の進歩に伴い，新しい機器や解析ソフトの開発や改良が急速に進み，胃用のカプセル内視鏡も開発中である．これらのカプセル内視鏡の発展に伴い，近い将来には消化器内視鏡検査全体が劇的に変化していくものと思われる．

文献

1) Iddan G, Merron G, Glukhovsky A et al : Wireless capsule endoscopy. Nature 405 : 417, 2000
2) 榊 信廣：カプセル内視鏡とは．カプセル内視鏡診療ガイド（カプセル内視鏡研究会編集，寺野彰監修)，南江堂，東京，2–7，2006
3) 中村哲也，生沼健司，山岸秀嗣，他：カプセル内視鏡（1）Given Imaging，早期大腸癌 11 : 183–189, 2007
4) 中村哲也，荒川哲男，後藤秀美，他：小腸用カプセル内視鏡の日本人における多施設共同研究報告—原因不明消化管出血を中心に—．Gastroenterol Endosc 49 : 324–334, 2007
5) Yamamoto H, Kita H, Sunada K et al : Clinical outcomes of double-balloon endoscopy for the diagnosis and treatment of small-intestinal disease. Clin Gastroenterol Hepatol 2 : 1010–1016, 2004
6) Rey JF, Ladas S, Alhassani A et al : European Society of Gastrointestinal Endoscopy (ESGE). Video capsule endoscopy: update to guidelines (May 2006). Endoscopy 38 : 1047–1053, 2006
7) Schoofs N, Deviére J, Van Gossum A : PillCam colon capsule endoscopy compared with colonos-

copy for colorectal tumor diagnosis: A prospective study. Endoscopy 38 : 963–968, 2006
8) Eliakim R, Fireman Z, Gralnek IM et al : Evaluation of the PillCam colon-capsule in the detection of colonic pathology: Results of the first multicenter, prospective, comparative study. Endoscopy 38 : 963–970, 2006

* * *

Determining the treatment strategy for colorectal neoplastic lesions: endoscopic assessment or the non-lifting sign for diagnosing invasion depth?

Authors N. Kobayashi[1,2], Y. Saito[1], Y. Sano[3], N. Uragami[4], T. Michita[5], J. Nasu[6], T. Matsuda[1], K. I. Fu[3], T. Fujii[7], T. Fujimori[8], T. Ishikawa[2], D. Saito[1]

Institutions Institutions are listed at the end of article.

submitted 31 October 2006
accepted after revision 15 March 2007

Bibliography
DOI 10.1055/s-2007-966587
Endoscopy 2007; 39: 701–705 © Georg Thieme Verlag KG Stuttgart · New York
ISSN 0013-726X

Corresponding author
N. Kobayashi, MD
Department of Diagnostic Imaging
Tochigi Cancer Center
Yonan 4-9-13
Utsunomiya
Tochigi 320-0834
Japan
Fax: +81-28-658-5488
nkobayas@tcc.pref.tochigi.jp

Background and study aims: Assessment of the invasion depth of colorectal neoplasia is important in deciding between endoscopic and surgical resection treatment methods. Prior to attempting endoscopic resection, the lesion is lifted by submucosal injection, and a positive "non-lifting sign" is usually considered to indicate deeper submucosal infiltration. The purpose of this prospective multicenter study was to assess the predictive value of the non-lifting sign for differentiating between adenoma and early cancer (up to discrete submucosal infiltration [sm1]) and cancer with deeper infiltration (sm2).

Patients and methods: During an 11-month period, a total of 271 colorectal neoplastic lesions in 239 patients were included in the study. Apart from the location, size, and macroscopic type of the lesion, the presence or absence of the non-lifting sign was recorded and compared with the endoscopic assessment of invasion depth.

Results: The non-lifting sign had a sensitivity of 61.5%, a specificity of 98.4%, a positive predictive value of 80.0%, a negative predictive value of 96.0%, and an accuracy of 94.8%. Endoscopic diagnosis of deeper infiltration had a sensitivity of 84.6%, a specificity of 98.8%, a positive predictive value of 88.0%, a negative predictive value of 98.4%, and an accuracy of 97.4%. Statistically significant differences were found in terms of sensitivity and accuracy.

Conclusion: Because of its lower sensitivity and accuracy, the non-lifting sign will not replace endoscopic assessment. If a lesion does not lift, this can make resection technically difficult, but does not reliably predict deeper cancerous invasion.

Introduction

In Japan submucosal cancers are subclassified into "sm1" cancers (where the distance from the muscularis mucosae to the deepest point of invasion is < 1 mm) and "sm2" cancers (where the distance from the muscularis mucosae to the deepest point of invasion is ≥ 1 mm). Because it is believed that sm1 lesions without lymphovascular involvement or a poorly differentiated component are rarely associated with lymph node metastasis, they are thought to be resectable endoscopically, in a similar manner to adenomas and intramucosal cancers [1,2]. In order to determine the appropriate treatment for colorectal neoplastic lesions, therefore, it is necessary to estimate whether or not the depth of invasion from the muscularis mucosae is less than 1 mm. Magnifying colonoscopy [3–9] and endoscopic ultrasound [9–13] have been reported to be helpful for this type of endoscopic assessment, although only experts are able to use these techniques adequately, and learning them requires considerable time and experience [14,15].

Endoscopic mucosal resection (EMR) is a safe technique for resecting large or flat colorectal neoplastic lesions after submucosal injection of liquid [16–18], and this submucosal injection is also thought to be useful for the diagnostic assessment of invasion depth [19–21]. Adenomas and intramucosal cancers are readily lifted by submucosal injection, in contrast to invasive cancer, which cannot be lifted because of submucosal fibrosis or desmoplastic change. Uno et al. [19] described this phenomenon as the "non-lifting sign", although their data were obtained at a single institution, about half of the cases they studied were small adenomas measuring less than 10 mm, and only 10 invasive cancers were evaluated. The usefulness of the non-lifting sign therefore still needs to be clarified.

The purpose of this prospective multicenter trial was to assess the accuracy of the non-lifting sign, in comparison with endoscopic diagnosis, as a diagnostic tool to determine whether or not the depth of invasion from the muscularis mucosae is less than 1 mm.

Patients and methods

This study was a prospective trial conducted at five medical centers in Japan between January 2004 and November 2004. Institutional review board approval was obtained at each participating institution, and informed written consent was obtained from all patients before the diagnostic and therapeutic procedures were carried out.

Eligibility and exclusion criteria

We included all colorectal neoplastic lesions except (a) lesions larger than 30 mm, (b) polypoid lesions smaller than 10 mm, (c) pedunculated polyps, (d) residual or recurrent lesions after endoscopic resection, and (e) colitis-associated lesions. Lesions diagnosed pathologically as colorectal cancer that had invaded beyond the submucosa (i.e. T2 or more) and non-neoplastic lesions were also excluded.

Endoscopic procedure

For colonic preparation all the centers used 2–3 liters of polyethylene glycol-electrolyte solution on the day of the procedure. All the patients received scopolamine butylbromide 20 mg intravenously unless this was contraindicated and sedation (for example with midazolam or diazepam) if required. All the investigators in this study had performed more than 500 colonoscopic procedures. When the eligible lesion was identified, its surface was washed with water before spraying 5 mL of 0.4% indigo carmine directly through the accessory channel of the scope. Each investigator diagnosed the depth of invasion after chromoscopic enhancement. Findings such as fold convergence, an expansive appearance, an irregular surface contour, a demarcated depressed area, or a large nodule (≥ 1 cm) in the flat lesion were regarded as signs of deep invasion [22–24]. Depending on the estimated depth of invasion, lesions were finally classified endoscopically as either "type A(e)" (sm2 cancers) or "type B(e)" (adenomas, intramucosal cancers, and sm1 cancers). On the basis of this endoscopic assessment, therefore, type A(e) lesions were considered to be candidates for surgical treatment and type B(e) lesions to be suitable for EMR. The location, size, and macroscopic type of the lesions were also recorded for analysis.

Submucosal injection

Submucosal injection was performed at a point approximately 2 mm from the edge of the lesion with a 23-gauge needle, and the frequency of injections was adjusted according to the size of the lesion. Normal saline or glycerol (Glyceol [10% glycerol and 5% fructose in normal saline solution]; Chugai Pharmaceutical Co., Tokyo, Japan) was used for the submucosal injection [25]. The non-lifting sign was defined (according to the criteria used by Uno et al. [19]) as positive when the surrounding mucosa, but not the lesion, was elevated, and negative when the lesion itself was elevated (**Fig. 1, 2**). The presence or absence of the non-lifting sign after submucosal injection was recorded for comparison with the endoscopic assessment of invasion depth.

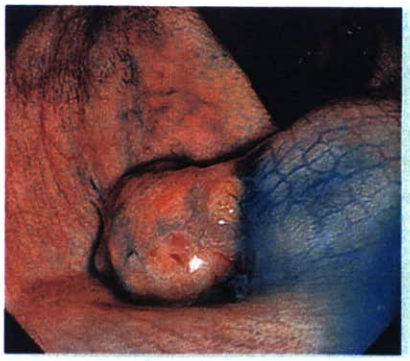

Fig. 1 Positive non-lifting sign: the submucosal injection has resulted in elevation of the mucosa surrounding the lesion, but not of the lesion itself.

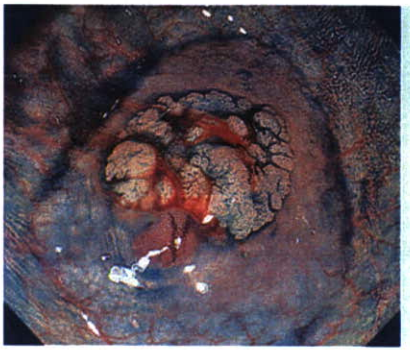

Fig. 2 Negative non-lifting sign: both the lesion and the surrounding mucosa were well elevated by the submucosal injection in this case.

Histopathological evaluation

Either EMR or surgical resection was performed for all lesions. All the specimens were fixed in 10% buffered formalin solution and stained with hematoxylin and eosin. All tissues were examined by the pathologists at each institution with reference to the Japanese classification of cancer of the colon and rectum [26]. The pathologists were all blinded to the endoscopic findings. The depth of invasion was classified histopathologically as either type A(h) (sm2 cancer) or type B(h) (adenoma, intramucosal cancer, or sm1 cancer).

Statistical analysis

The aim of this study was to assess the sensitivity and specificity of the non-lifting sign for distinguishing sm2 cancer from adenoma, intramucosal cancer, and sm1 cancer. A high specificity was considered to be necessary because it is important that patients avoid unnecessary surgery. We therefore assumed a specificity of 95%, with a 95% confidence interval (CI) of ± 3%, to decide on the sample size required for this study, and it was calculated that a total enrollment of 200 lesions would be needed.

All values are reported as means ± standard deviation when applicable. The accuracy, sensitivity, specificity, positive predictive value (PPV), negative predictive value (NPV), and accuracy were evaluated by comparing the results for the non-lifting sign or endoscopic diagnosis with the histopathological diagnosis. Comparisons were made using McNemar's test or Fisher's exact test. Probability values of less than 0.05 were considered to signify statistical significance. All calculations were performed using the SPSS statistical software package (SPSS, Chicago, Illinois, USA).

Results

At the time of the endoscopic procedures, 252 patients with 284 lesions were initially enrolled in this study. After histological evaluation, eight deep invasive colorectal cancers (T2) and five

Total number of lesions	271
Location, n (%)	
Rectum	55 (20.3%)
Distal colon	108 (39.9%)
Proximal colon	108 (39.9%)
Size, n (%)	
≤ 10 mm	135 (49.8%)
11 – 20 mm	122 (47.2%)
21 – 30 mm	14 (5.2%)
Mean size ± standard deviation, mm	12.3 ± 5.4
Macroscopic type, n (%)	
Polypoid	89 (32.8%)
Flat and depressed	182 (67.2%)
Histopathological type, n (%)	
Type A(h) lesions (sm2 cancer)	26 (9.6%)
Type B(h) lesions	245 (90.4%)
Adenoma	161 (59.4%)
Intramucosal cancer	72 (26.6%)
sm1 cancer	12 (4.4%)

Table 1 The clinicopathological characteristics of the lesions included in the study

non-neoplastic lesions were excluded from the analysis, and so 271 lesions in 239 patients were finally included in the study. The clinicopathological characteristics of these lesions are summarized in **Table 1**.

The non-lifting sign as a diagnostic tool

The overall accuracy of the non-lifting sign as a tool for determining the depth of invasion was 94.8% (257/271), and its sensitivity, specificity, PPV, and NPV were 61.5% (16/26), 98.4% (241/245), 80.0% (16/20), and 96.0% (241/251) respectively (**Table 2**). On the basis of the macroscopic type, the accuracy, sensitivity, specificity, PPV, and NPV of the non-lifting sign were 95.5% (85/89), 55.6% (5/9), 100% (80/80), 100% (5/5), and 95.2% (80/84) respectively for polypoid lesions (**Table 3**), and 94.5% (172/182), 64.7% (11/17), 97.6% (161/165), 73.3% (11/15), and 96.4% (161/167) respectively for flat and depressed lesions (**Table 4**).

Accuracy of endoscopic diagnosis vs. the non-lifting sign

The results for the overall accuracy, sensitivity, specificity, PPV value, and NPV of endoscopic diagnosis were 97.4% (264/271), 84.6% (22/26), 98.8% (242/245), 88.0% (22/25), and 98.4% (242/246) respectively (**Table 2**). The specificity of endoscopic diagnosis was similar to that of the non-lifting sign, but the sensitivity and accuracy of endoscopic diagnosis were significantly higher than the sensitivity and accuracy of the non-lifting sign ($P = 0.031$ for the difference in sensitivity and $P = 0.039$ for the difference in accuracy). On the basis of the macroscopic type, the results for the accuracy, sensitivity, specificity, PPV, and NPV of endoscopic diagnosis of polypoid lesions were 96.6% (86/89), 66.7% (6/9), 100% (80/80), 100% (6/6), and 96.4% (80/83), respectively (**Table 3**). For flat and depressed-type lesions, endoscopic diagnosis showed an accuracy of 97.8% (178/182), a sensitivity of 94.1% (16/17), a specificity of 98.2% (162/165), a PPV of 84.2% (16/19), and an NPV of 99.4% (162/163) (**Table 4**). The sensitivity and accuracy of endoscopic diagnosis for flat and depressed lesions were also higher than the sensitivity and accuracy of the non-lifting sign, although not to a significant degree ($P = 0.063$ for the difference in sensitivity and $P = 0.07$ for the difference in accuracy) (**Table 5**).

Glycerol vs. normal saline for assessment of the non-lifting sign

Glycerol was used as the injection agent for 219 lesions (80.8%), and normal saline for 52 lesions (19.2%). Of the 26 sm2 cancers, 19 were included in the glycerol-injection group, and 10 of these showed the non-lifting sign. The remaining seven sm2 cancers were included in the normal saline-injection group, and six of these showed the non-lifting sign. The accuracy, sensitivity, and specificity of the non-lifting sign in the glycerol-injection lesions were 95.0% (208/219), 52.6% (10/19), and 99.0% (198/200) respectively; the accuracy, sensitivity, and specificity of the non-lifting sign in the normal saline-injection lesions were

	Non-lifting sign		Endoscopic diagnosis	
	Positive	Negative	Type A(e)	Type B(e)
Histopathology				
Type A(h) lesions	16	10	22	4
Type B(h) lesions	4	241	3	242
Sensitivity	61.5%(16/26)		84.6% (22/26)	
Specificity	98.4% (241/245)		98.8% (242/245)	
Positive predictive value	80.0% (16/20)		88.0% (22/25)	
Negative predictive value	96.0% (241/251)		98.4% (242/246)	
Accuracy	94.8% (257/271)		97.4% (264/271)	

Table 2 The non-lifting sign vs. endoscopic assessment in the diagnosis of all 271 lesions, where type A lesions were sm2 cancers and type B lesions were adenomas, intramucosal cancers, or sm1 cancers

	Non-lifting sign		Endoscopic diagnosis	
	Positive	Negative	Type A(e)	Type B(e)
Histopathology				
Type A(h) lesions	5	4	6	3
Type B(h) lesions	0	80	0	80
Sensitivity	55.6% (5/9)		66.7 (6/9)	
Specificity	100% (80/80)		100% (80/80)	
Positive predictive value	100% (5/5)		100% (6/6)	
Negative predictive value	95.2% (80/84)		96.4% (80/83)	
Accuracy	95.5% (85/89)		96.6% (86/89)	

Table 3 The non-lifting sign vs. endoscopic assessment in the diagnosis of the 89 polypoid lesions, where type A lesions were sm2 cancers and type B lesions were adenomas, intramucosal cancers, or sm1 cancers

	Non-lifting sign		Endoscopic diagnosis	
	Positive	Negative	Type A(e)	Type B(e)
Histopathology				
Type A(h) lesions	11	6	16	1
Type B(h) lesions	4	161	3	162
Sensitivity	64.7% (11/17)		94.1% (16/17)	
Specificity	97.6% (161/165)		98.2% (162/165)	
Positive predictive value	73.3% (11/15)		84.2% (16/19)	
Negative predictive value	96.4% (161/167)		99.4% (162/163)	
Accuracy	94.5% (172/182)		97.8% (178/182)	

Table 4 The non-lifting sign vs. endoscopic assessment in the diagnosis of the 182 flat and depressed-type lesions, where type A lesions were sm2 cancers and type B lesions were adenomas, intramucosal cancers, or sm1 cancers

	Non-lifting sign	Endoscopic diagnosis	*P*
All lesions (n = 271)			
Sensitivity	61.5%	84.6%	0.031
Specificity	98.4%	98.8%	1.0
Postitive predictive value	80.0%	88.0%	0.682
Negative predictive value	96.0%	98.4%	0.174
Accuracy	94.8%	97.4%	0.039
Polypoid lesions (n = 89)			
Sensitivity	55.6%	66.7%	1.0
Specificity	100%	100%	–
Positive predictive value	100%	100%	–
Negative predictive value	95.2%	96.4%	1.0
Accuracy	95.5%	96.6%	1.0
Flat and depressed lesions (n = 182)			
Sensitivity	64.7%	94.1%	0.063
Specificity	97.6%	98.2%	1.0
Positive predictive value	73.3%	84.2%	0.672
Negative predictive value	96.4%	99.4%	0.121
Accuracy	94.5%	97.8%	0.07

Table 5 The non-lifting sign vs. endoscopic diagnosis: summary

94.2% (49/52), 85.7% (6/7), and 95.6% (43/45) respectively. Although the sensitivity of the non-lifting sign tended to be higher in the lesions that had been injected with normal saline than it was in the lesions injected with glycerol, there was no significant difference between normal saline injection and glycerol injection in terms of the accuracy, sensitivity, or specificity of the non-lifting sign.

Outcome of EMR

No complication associated with either submucosal injection or the EMR occurred during or immediately after the procedure. Of the 10 sm2 cancers that were negative for the non-lifting sign, four were resected by EMR. One of these four lesions was found to have a positive vertical margin pathologically, but additional surgery revealed no local recurrence and no lymph-node or distant metastasis.

Discussion

This study is the first prospective multicenter investigation of the non-lifting sign as a tool for determining the depth of invasion of colorectal neoplastic lesions. Our findings revealed that the non-lifting sign alone was not enough for making an accurate diagnosis of sm2 cancer. It resulted in an increased frequency of unnecessary EMR for sm2 cancer, which had to be followed by additional surgery. On the basis of the morphology, the accuracy of the non-lifting sign and the accuracy of endoscopic diagnosis were almost the same for polypoid lesions, but the sensitivity of the non-lifting sign was inferior to that of endoscopic diagnosis for flat and depressed lesions. This suggests that endoscopic diagnosis is more reliable, especially for flat and depressed lesions. On the other hand, the accuracies of both methods were insufficient for determining the depth of invasion of polypoid lesions. Currently, to prevent unnecessary surgery, it appears that polypoid lesions that are negative for the non-lifting sign should be resected by EMR.

Uno et al. [19] defined the non-lifting sign as an indicator of invasive cancer. They evaluated 193 neoplastic lesions, and reported that the sensitivity and specificity of the non-lifting sign were as high as 100% and 99%, respectively. In our opinion, the higher sensitivity and specificity results obtained in their study might have resulted from the limited number of invasive cancers they included (only 10, including four submucosal cancers). In contrast, because we included 38 submucosal cancers and excluded advanced cancers (e.g. tumors that were T2 or more), our sensitivity result was lower than theirs. Nevertheless, we consider that our results reflect the clinical situation more precisely because we prospectively evaluated all colorectal neoplastic lesions detected by colonoscopy. In addition, the solutions used for the submucosal injection were different in the two studies. We used mainly glycerol because this makes EMR technically easier [25]. In our study there were no significant differences in the accuracy, sensitivity, and specificity of the non-lifting sign between lesions lifted by glycerol and lesions lifted using normal saline, although the sensitivity in the glycerol group tended to be inferior to that in the normal saline group. In order to clarify whether or not the use of glycerol or normal saline influences

the frequency of non-lifting-sign positivity, an additional comparative study using a prospective design is mandatory.

Because our study was conducted at five medical centers that specialize in endoscopy, the accuracy of endoscopic diagnosis in this study could be considered to be representative of that of experienced Japanese colonoscopists. In general, endoscopic diagnosis is comparatively subjective, and probably depends to a great extent on the ability of the individual examiner. However, this issue has received little attention in clinical studies. Because both of these diagnostic modalities might depend on the ability of the investigator, it is still uncertain to what extent inexperience affects the results. For inexperienced colonoscopists, the non-lifting sign may be easier to learn than precise endoscopic diagnosis. The learning curves of endoscopic diagnosis and submucosal injection should be investigated to clarify this issue. However, the present results suggest that the non-lifting sign cannot replace endoscopic diagnosis by experienced colonoscopists.

In conclusion, although the non-lifting sign showed high specificity, its sensitivity and accuracy are insufficient in comparison with endoscopic diagnosis for diagnosing invasion depth. If colonoscopists are experienced, the non-lifting sign is not as efficient as endoscopic diagnosis for determining the appropriate treatment for colorectal neoplastic lesions. Further studies of interexaminer variation and the learning curves for each method are necessary so that these results can be adjusted to reflect the experience of all colonoscopists.

Acknowledgments

This work was supported in part by the Grant-in-aid for Cancer Research (18S-2) from the Ministry of Health, Labour and Welfare. We would like to thank Yoshitaka Murakami from the Department of Health Science at Shiga University of Medical Science for his valuable advice on the statistical analysis.

Competing interests: None

Institutions

[1] Division of Endoscopy, National Cancer Center Hospital, Tokyo, Japan
[2] Department of Diagnostic Imaging, Tochigi Cancer Center, Tochigi, Japan
[3] Department of Endoscopy, National Cancer Center Hospital East, Chiba, Japan
[4] Department of Gastroenterology, Cancer Insutitute Hospital, Tokyo, Japan
[5] Department of Gastroenterology, Osaka National Hospital, Osaka, Japan
[6] Department of Internal Medicine, National Hospital Organization Shikoku Cancer Center, Ehime, Japan
[7] TF Clinic, Tokyo, Japan
[8] Department of Surgical and Molecular Pathology, Dokkyo University School of Medicine, Tochigi, Japan

References

1 *Kitajima K, Fujimori T, Fujii S et al.* Correlations between lymph node metastasis and depth of submucosal invasion in submucosal invasive colorectal carcinoma: a Japanese collaborative study. J Gastroenterol 2004; 39: 534–543
2 *Participants in the Paris Workshop.* The Paris endoscopic classification of superficial neoplastic lesions: esophagus, stomach and colon. November 30 to December 1, 2002. Gastrointest Endosc 2003; 58: S3–S43
3 *Kudo S, Tamura S, Nakajima T et al.* Diagnosis of colorectal tumorous lesions by magnifying endoscopy. Gastrointest Endosc 1996; 44: 8–14
4 *Kudo S, Rubio CA, Teixeira CR et al.* Pit pattern in colorectal neoplasia: endoscopic magnifying view. Endoscopy 2001; 33: 367–373
5 *Fujii T, Hasegawa RT, Saitoh Y et al.* Chromoscopy during colonoscopy. Endoscopy 2001; 33: 1036–1041
6 *Kato S, Fujii T, Koba I et al.* Assessment of colorectal lesions using magnifying colonoscopy and mucosal dye-spraying: can significant lesions be distinguished? Endoscopy 2001; 33: 306–310
7 *Matsuda T, Fujii T, Ono A et al.* Effectiveness of magnifying colonoscopy in diagnosing the depth of invasion of colorectal neoplastic lesions: invasive pattern is an indication for surgical treatment. Gastrointest Endosc 2003; 575: AB176
8 *Hurlstone DP, Brown S, Cross SS et al.* High magnification chromoscopic colonoscopy or high frequency 20 MHz mini probe endoscopic ultrasound staging for early colorectal neoplasia: a comparative prospective analysis. Gut 2005; 54: 1585–1589
9 *Hurlstone DP, Cross SS, Adam I et al.* Endoscopic morphological anticipation of submucosal invasion in flat and depressed colorectal lesions: clinical implications and subtype analysis of the kudo type V pit pattern using high-magnification-chromoscopic colonoscopy. Colorectal Dis 2004; 6: 369–375
10 *Matsumoto T, Hizawa K, Esaki M et al.* Comparison of EUS and magnifying colonoscopy for assessment of small colorectal cancers. Gastrointest Endosc 2002; 56: 354–360
11 *Hizawa K, Suekane H, Aoyagi K et al.* Use of endosonographic evaluation of colorectal tumor depth in determining the appropriateness of endoscopic mucosal resection. Am J Gastroenterol 1996; 91: 768–771
12 *Cho E, Nakajima M, Yasuda K et al.* Endoscopic ultrasonography in the diagnosis of colorectal cancer invasion. Gastrointest Endosc 1993; 39: 521–527
13 *Tio TL, Weijers O, Hulsman F et al.* Endosonography of colorectal diseases. Endoscopy 1992; 24: 309–314
14 *Togashi K, Konishi F, Ishizuka T et al.* Efficacy of magnifying endoscopy in the differential diagnosis of neoplastic and non-neoplastic polyps of large bowel. Dis Colon Rectum 1999; 42: 1602–1608
15 *Kobayashi N, Matsuda T, Saito Y et al.* Is pit pattern diagnosis possible even for beginners? Gastrointest Endosc 2004; 59: AB123
16 *Karita M, Tada M, Okita K et al.* Endoscopic therapy for early colon cancer: the strip biopsy resection technique. Gastrointest Endosc 1991; 37: 128–132
17 *Kudo S, Tamegai Y, Yamano H et al.* Endoscopic mucosal resection of the colon: the Japanese technique. Gastrointest Endosc Clin N Am 2001; 11: 519–535
18 *Soetikno RM, Gotoda T, Nakanishi Y et al.* Endoscopic mucosal resection. Gastrointest Endosc 2003; 57: 567–579
19 *Uno Y, Munakata A.* The non-lifting sign of invasive colon cancer. Gastrointest Endosc 1994; 40: 485–489
20 *Kato H, Haga S, Endo S et al.* Lifting of lesions during endoscopic mucosal resection (EMR) of early colorectal cancer: implications for the assessment of resectability. Endoscopy 2001; 33: 568–573
21 *Ishiguro A, Uno Y, Ishiguro Y et al.* Correlation of lifting versus non-lifting and microscopic depth of invasion in early colorectal cancer. Gastrointest Endosc 1999; 50: 329–333
22 *Saitoh Y, Obata T, Watari J et al.* Invasion depth diagnosis of depressed type early colorectal cancers by combined use of videoendoscopy and chromoendoscopy. Gastrointest Endosc 1998; 48: 362–370
23 *Saitoh Y, Watari J, Fujitani M et al.* Diagnostic accuracy of the submucosal invasion depth for colorectal submucosal cancers, diagnosis of submucosal invasion depth 1,000 μm by conventional colonoscopy [in Japanese, English abstract]. Stomach Intestine 2004; 39: 1350–1356
24 *Uraoka T, Saito Y, Matsuda T et al.* Endoscopic indications for endoscopic mucosal resection of laterally spreading tumours in the colorectum. Gut 2006; 55: 1592–1597
25 *Uraoka T, Fujii T, Saito Y et al.* Effectiveness of glycerol as a submucosal injection for EMR. Gastrointest Endosc 2005; 61: 736–740
26 *Japanese Research Society for Cancer of the Colon and Rectum.* General rules for clinical and pathological studies on cancer of the colon, rectum and anus: histopathological classification. 6th edn. Tokyo: Kanehara Syuppan, 1998: 60–90

Abnormal serum liver chemistry related to pneumoperitoneum after endoscopic submucosal dissection

A 61-year-old man had been followed after endoscopic submucosal dissection (ESD) for early gastric cancer. In his youth, the patient had undergone total colectomy because of Crohn's disease. Surveillance esophagogastroduodenoscopy revealed metachronous early gastric cancer, so a second ESD was performed. Although gastric perforation occurred during the procedure, it was closed completely using endoclips (**Fig. 1** and **2**). Antibiotic therapy was started with fasting. The following day, 12 h after the second ESD, laboratory data included aspartate aminotransferase 225 U/L (normal range 12–32 U/L), alanine aminotransferase 201 U/L (2–38 U/L), lactate dehydrogenase 526 U/L (119–229 U/L), creatine phosphokinase 512 U/L (40–218 U/L), C-reactive protein 3.47 mg/dl (< 0.3 mg/dl), and white blood cell count 27.75 × 10^3/L (3.4–9.4 × 10^3/L). As electrocardiography and troponin test ruled out ischemic heart disease, an effect of pneumoperitoneum was strongly suspected. An abdominal CT scan showed severe pneumoperitoneum with compression of the inferior vena cava (**Fig. 3**), and therefore abdominal decompression with a 14-gauge puncture needle was performed. Immediately after the puncture, the abdominal fullness and back pain improved. Four days later, almost all of the laboratory parameters recovered to within the normal ranges, and the patient made an uneventful recovery during the 14 months of follow-up after the procedure.

Gastric perforation is a major complication of endoscopic treatment, but most perforations are small and can be managed endoscopically using endoclips [1,2]. After endoscopic closure, if severe abdominal fullness persists, needle puncture is performed for decompression of the pneumoperitoneum in order to prevent negative systemic effects. It has been reported that prolonged pneumoperitoneum increases main arterial blood pressure and systemic vascular resistance but decreases stroke volume and cardiac output during laparoscopic surgery with carbon dioxide insufflation [3,4]. In our patient, abdominal CT scan revealed compression of the inferior vena cava, suggesting high intra-abdominal pressure. In this condition, we believe that the increased main arterial blood pressure and systemic vascular resistance caused congestion of the liver, resulting in elevation of liver enzyme levels [5].

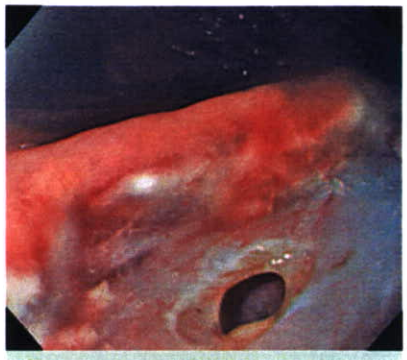

Fig. 1 Gastric perforation occurred during ESD.

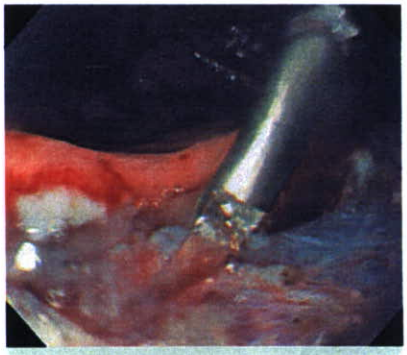

Fig. 2 Endoscopic closure was performed using an endoclip.

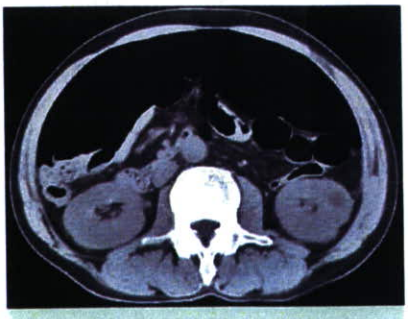

Fig. 3 Abdominal CT scan showed severe pneumoperitoneum and compression of the inferior vena cava.

Acknowledgment

This work was supported in part by a Grant-in-Aid for Cancer Research (18S-2) from the Ministry of Health, Labour and Welfare.

Endoscopy_UCTN_Code_CPL_1AH_2AZ

N. Kobayashi[1], T. Ishikawa[1], K.-I. Fu[2], T. Yamamoto[1], Y. Hirahara[1], R. Sekiguchi[1]

[1] Department of Diagnostic Imaging, Tochigi Cancer Center, Tochigi, Japan

[2] Department of Radiology, Dokkyo University School of Medicine, Tochigi, Japan

References

1 *Minami S, Gotoda T, Ono H et al.* Complete endoscopic closure of gastric perforation induced by endoscopic resection of early gastric cancer using endoclips can prevent surgery (with video). Gastrointest Endosc 2006; 63: 596–601

2 *Oda I, Gotoda T, Hamanaka H et al.* Endoscopic submucosal dissection for early gastric cancer: technical feasibility, operation time and complications from a large consecutive series. Dig Endosc 2005; 17: 54–58

3 *Koivusalo AM, Lindgren L.* Effects of carbon dioxide pneumoperitoneum for laparoscopic cholecystectomy. Acta Anaesthesiol Scand 2000; 44: 834–841

4 *McLaughlin JG, Scheeres DE, Dean RJ et al.* The adverse hemodynamic effects of laparoscopic cholecystectomy. Surg Endosc 1995; 9: 121–124

5 *Meierhenrich R, Gauss A, Vandenesch P et al.* The effects of intraabdominally insufflated carbon dioxide on hepatic blood flow during laparoscopic surgery assessed by transesophageal echocardiography. Anesth Analg 2005; 100: 340–347

Bibliography

DOI 10.1055/s-2007-966818

Endoscopy 2007; 39: E327

ISSN 0013-726X

Corresponding author

N. Kobayashi, MD

Department of Diagnostic Imaging
Tochigi Cancer Center
320-0834 Yonan
Utsunomiya
Tochigi
Japan
Fax: +81-28-6585488
nkobayas@tcc.pref.tochigi.jp

H

Magn Reson Med Sci, Vol. 6, No. 2, pp. 61–66, 2007

MAJOR PAPER

Hypointensity on Postcontrast MR Imaging from Compression of the Sacral Promontory in Enlarged Uterus with Huge Leiomyoma and Adenomyosis

Kensuke UOTANI[1,2*], Shuichi MONZAWA[1], Shuji ADACHI[1], Masayuki TAKEMORI[3], Yasushi KAJI[4], and Kazuro SUGIMURA[2]

Departments of [1]Radiology and [3]Gynecology, Hyogo Medical Center for Adults
[2]Department of Radiology, Kobe University Graduate School of Medicine
7-5-2, Kusunoki-cho, Chuo-ku, Kobe, Hyogo 650-0017, Japan
[4]Department of Radiology, Dokkyo University School of Medicine
(Received March 22, 2006; Accepted March 28, 2007)

Purpose: In patients with huge leiomyoma and with adenomyosis of the uterus, a peculiar area of hypointensity was occasionally observed on postcontrast magnetic resonance (MR) imaging in the dorsal portion of the enlarged uterus near the sacral promontory. We describe the imaging characteristics of these MR findings and correlate them with histopathological findings to examine whether the areas represent specific pathological changes.

Methods: Ten patients with huge leiomyomas and two with huge adenomyotic lesions whose imaging revealed the hypointensity were enrolled. All had enlarged uteri that extended beyond the sacral promontory. MR findings of the hypointense areas were evaluated and correlated with histopathological findings in 5 patients with leiomyoma and two with adenomyosis who had hysterectomy.

Results: The ten patients with leiomyoma showed flare-shaped hypointensity arising from the dorsal surface of the uterine body that extended deep into the tumor. The base of the hypointense areas was narrow in 5 patients with intramural leiomyoma and broad in five with subserosal leiomyoma. Two patients with adenomyosis showed nodular-shaped areas of hypointensity in front of the sacral promontory. Precontrast T_1- and T_2-weighted MR images showed no signal abnormalities in the portions corresponding to the hypointensity in any of the 12 patients. Pathological examinations showed no specific findings in the portions corresponding to the hypointensity in the 7 patients who had hysterectomy.

Conclusion: The areas of hypointensity may represent functional changes, such as decreased localized blood flow caused by compression of the sacral promontory.

Keywords: *uterus, leiomyoma, adenomyosis, pseudolesion, MRI*

Introduction

Uterine leiomyomas are common benign tumors composed of bundles of proliferated smooth muscle cells and are seen in women of child-bearing age.[1] They usually show homogeneous decreased signal intensity on T_1- and T_2-weighted MR images from relaxation times of smooth muscle[2] and homogeneous enhancement on postcontrast T_1-weighted MR images. Leiomyomas may show varying degrees of degeneration, and degenerated leiomyomas tend to demonstrate inhomogeneous signal intensity on T_2-weighted MR images and inhomogeneous enhancement on postcontrast T_1-weighted images.[3]

Park and associates[4] reported 3 patients with huge leiomyoma who showed geographic hypointense areas that mimicked degeneration near the sacral promontory on postcontrast T_1-weighted MR images. Precontrast T_1- and T_2-weighted MR images showed no signal abnormalities at the sites corresponding to hypointensity. They found no pathological changes, such as necrosis or degeneration, in surgical specimens and therefore thought that the hypotensity represented functional changes. We observed similar findings in patients with huge leiomyomas and patients with adenomy-

*Corresponding author, Phone: +81-78-382-6104, Fax: +81-78-382-6129, E-mail: uota2@med.kobe-u.ac.jp

osis. To our knowledge, no detailed studies have described this curious finding, and the occurrence of such areas of hypointensity has not been reported in patients with adenomyosis. We describe MR imaging features of these areas and differences between hypointense areas with leiomyoma and with adenomyosis and correlate MR and histpathological findings to examine whether the areas represent specific pathological changes.

Material and Methods

A review of the radiological reports of 1479 pelvic MR imaging studies performed between April 2000 and October 2003 showed ten women (aged 27 to 53 years, mean 40 years) with huge leiomyoma and two with huge adenomyosis lesion whose postcontrast T_1-weighted MR images revealed the area of hypointensity. Diagnosis was confirmed by operation in 5 patients with leiomyoma and two with adenomyosis. MR examinations were performed within 4 months of surgery, and none of the seven received hormonal treatments prior to operation. In the other 5 patients, a well circumscribed mass of homogeneous decreased signal intensity with whorl-like high signal intensity was seen on T_2-weighted images, and leiomyoma was diagnosed on the basis of this typical MR finding. Malignancy was ruled out by follow-up imaging studies for a period of one year or more.

MR imaging was performed with Signa Horizon 1.5T or Signa Twin Speed 1.5T (GE Medical Systems, U.S.A.) using a torso or pelvic phased-array coil. An antiperistaltic drug (Buscopan; Boehringer Ingelheim, Japan) was given intramuscularly to minimize artifacts caused by bowel movement, and a band was fastened tightly on the hypogastrium to diminish artifacts from respiratory movement. T_1-weighted spin-echo MR images (repetition time/echo time, 500/8) and fat-saturated T_2-weighted fast spin-echo MR images (4000/100) were obtained in sagittal and axial planes with 24- to 32-cm field of view, 512×224 to 256 image matrix, 8-mm slice thickness, 2-mm gap, and one or 2 numbers of signal excitation. After precontrast imaging, 15 mL of gadopentetate dimeglumine (Magnevist®; Nihon Schering, Japan) were injected intravenously, and T_1-weighted spin-echo MR images, with or without fat saturation, were obtained using the same imaging parameters in axial, sagittal, and coronal planes.

Two radiologists (K.U. and S.M.) well experienced in MR imaging reviewed images in the 12 patients and evaluated the location and size of the leiomyomas and adenomyotic lesions. The number, shape, and size of the hypointense areas seen on postcontrast T_1-weighted MR images near the sacral promontory in the uterus were studied. The areas were classified as either flare-shaped with narrow base, flare-shaped with broad base, or nodular-shaped. Areas of hypointensity that arose from the dorsal surface of the uterine body and extended deeply and somehow radially were considered flare-shaped. Broad- and narrow-based subtypes were determined by the width of base at the dorsal surface of the uterus. Hypointense areas with relatively well-defined margins with less irregularity than those with flare shape were considered to be nodular in shape. Sagittal MR images were used to measure the areas, and precontrast T_1- and T_2-weighted MR images were studied to find signal abnormalities corresponding to the hypointense areas seen on postcontrast MR images.

MR findings were correlated with histopathological findings in 5 patients with huge leiomyoma and two with adenomyosis who underwent hysterectomy. In one patient with leiomyoma, the portion compressed by the sacral promontory was identified and marked with a stitch during the operation, and specimens obtained from that area underwent microscopic examination. In the other patients, pathological examinations were performed mainly by gross inspection on cut surface.

Results

Leiomyomas (maximum diameter, 70 to 140 mm; mean, 104.1 mm) were located in the subserosa of the dorsal body of the uterus in five of the 10 patients and in the myometrium of the dorsal body of the uterus in the remaining five. Adenomyotic lesions in the 2 patients measured 115 and 120 mm in maximum diameter. MR images of all twelve showed enlarged uterus that extended beyond the sacral promontory as a result of the disease. The dorsal surface of the uterus was depressed by compression of the sacral promontory.

Postcontrast T_1-weighted MR images of the 10 patients with huge leiomyoma showed one or 2 flare-shaped areas of hypointensity in the uterus near the sacral promontory. The areas were flare-shaped with broad base in the 5 patients with subserosal leiomyoma (Fig. 1) and flare-shaped with narrow base in the five with intramural leiomyoma (Fig. 2). In eight of the 10 patients with leiomyoma, a hypointense area was seen in front of the sacral promontory. In the other two, a hypointense area was seen in front of the fifth vertebra, not the promontory, in one and at the level of the fourth/fifth intervertebral space and extended caudally to

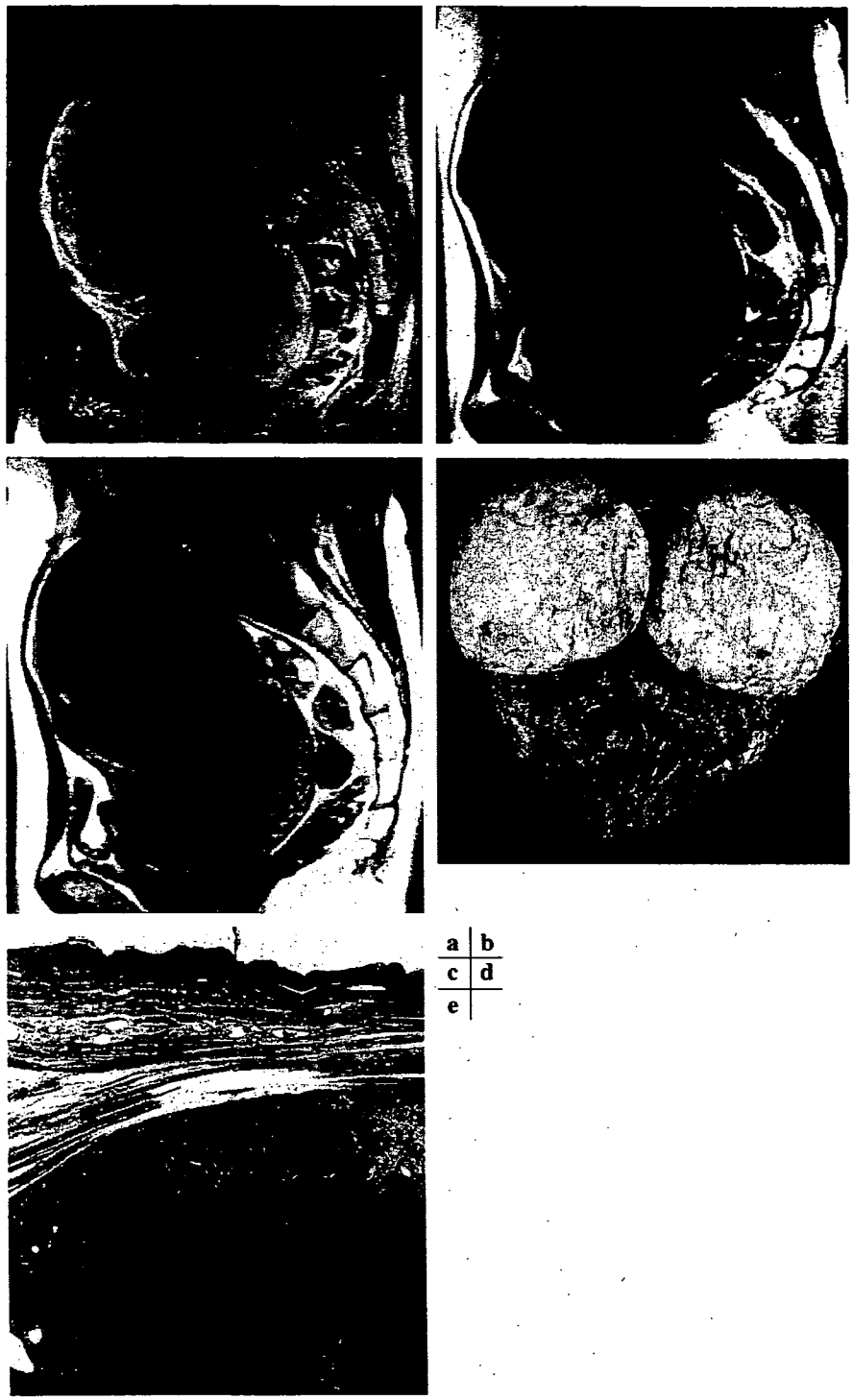

Fig. 1. A 46-year-old woman with a huge subserosal leiomyoma. Postcontrast T_1-weighted sagittal magnetic resonance (MR) image with fat saturation (**a**) shows a flare-shaped area of hypointensity in the dorsal portion of a leiomyoma. The area arises from the portion depressed by the sacral promontory and extends into the tumor. Precontrast T_1-weighted sagittal MR image (**b**) and T_2-weighted sagittal MR image (**c**) show no specific signal changes that correspond to the area seen in (**a**). Gross specimen (**d**) shows an indentation (arrows) compressed by the sacral promontory in a subserosal leiomyoma with moderate hyalinization. Microscopic specimen (**e**) obtained from the indented portion seen in (**d**) shows no specific findings, such as degeneration or necrosis.

Fig. 2. A 32-year-old woman with a huge intramural leiomyoma. Postcontrast T_1-weighted sagittal MR image with fat saturation (**a**) shows flare-shaped hypointensity in a leiomyoma. The base of the area involves normal myometrium between the tumor and sacral promontory, and compared to the base of hypointense areas seen in Fig. 1, it is narrow. T_2-weighted sagittal MR image (**b**) shows no specific signal changes corresponding to the area seen in (**a**).

the sacral promontory in the other. Maximum diameters of the areas ranged from 15 to 80 mm, with a mean of 42.5 mm. On precontrast T_1- and T_2-weighted MR images in all 10 patients with leiomyoma, no specific signal changes were noted at the sites corresponding to hypointensity. Postcontrast T_1-weighted MR images in 2 patients with adenomyosis showed nodular-shaped hypointensity (maximum diameter, 25 to 40 mm; mean, 33 mm) in front of the sacral promontory (Fig. 3). Precontrast T_1- and T_2-weighted MR images showed no signal abnormalities in the portions corresponding to these areas.

Histopathological studies in 4 patients showed subserosal tumor to be hyalinized or usual leiomyoma; an intramural tumor in one patient was a cellular leiomyoma, and adenomyosis seen in 2 patients was of a usual type. There was no specific degeneration or necrosis in these lesions at the site corresponding to the hypointensity. The findings of MR imaging and histopathological studies are summarized in Table.

Discussion

The hypointense areas observed in the 12 patients were thought to be identical to the geographic hypointense areas reported by Park and associates,[4] who also found no signal abnormalities on precontrast T_1- and T_2-weighted MR images that corresponded to the hypointensity. Histopathological examinations of the surgical specimens obtained from the 7 patients showed no specific pathological changes, such as degeneration or necrosis, at the corresponding sites. Based on these findings, we thought that a localized decrease in blood flow from compression of the sacral promontory caused diminished enhancement, and we agreed with the Park's conclusion. Although we did not perform delayed postcontrast imaging, Park's group found that the hypointense area disappeared on delayed MR images.

A similar phenomenon can be observed in the liver. Yoshimitsu and colleagues reported pseudolesions caused by rib compression.[5] On dynamic computed tomography (CT), compressed liver parenchyma just beneath the rib showed low attenuation on early-phase images, and the hypoattenuating area disappeared on delayed-phase images. They studied the pseudolesions using CT during arterial portography and during hepatic arteriography and showed that the compression caused by curved ribs could cause transient focal diminishment of portal venous perfusion without altering hepatic arterial perfusion in the liver parenchyma.

Pathologically, vascular density is less, the vascular network sparser, and the diameter of blood vessels is greater in tumor tissues of leiomyomas than in the myometrium.[6-8]

Adenomyosis is composed of ectopic endometrial glands and stroma that interdigitate with underlying myometrium,[9] and on angiography and histology, it has been described as having an arterial network that is less dense than that of adjacent myometrium.[10] Therefore, compared with tissues

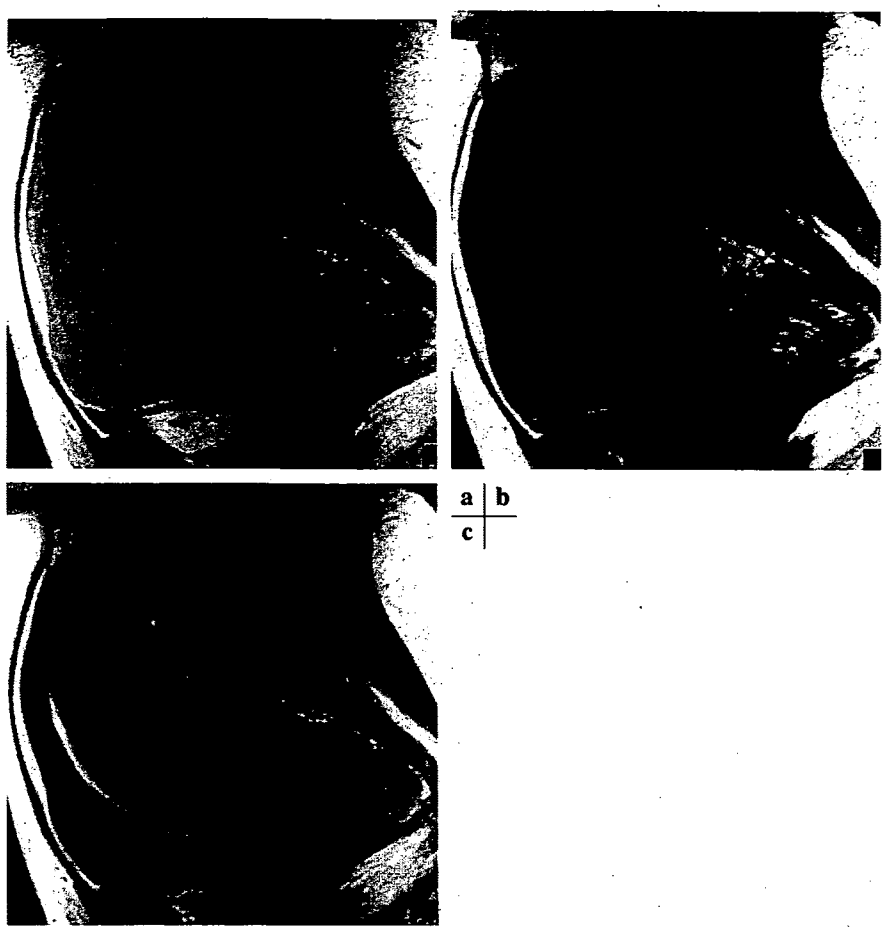

Fig. 3. A 48-year-old woman with huge adenomyosis. Postcontrast T_1-weighted sagittal MR image (**a**) shows nodular-shaped hypointensity in the portion compressed by the sacral promontory. Compared with hypointense areas seen in patients with leiomyoma (Figs. 1 and 2), the margin is less irregular and relatively well defined. Precontrast T_1-weighted sagittal MR image (**b**) and T_2-weighted sagittal image (**c**) show no specific signal changes that correspond to the area seen in (**a**).

of the myometrium, tissue of leiomyoma and adenomyosis may have impaired vasculature, and subsequent decrease in blood flow might readily occur. deSousa's group reported that perfusion was retained in the myometrium, but virtually stopped in leiomyoma on dynamic MR imaging performed immediately after bilateral uterine arterial embolization (UAE).[11] This result supports the idea mentioned previously.

In patients with leiomyoma, areas of hypointensity showed irregular margins shaped like a flare, especially on the deep side. Blood vessels within leiomyomas orient in the direction of muscle cell bundles that show a whorl-like pattern,[6,7] so the irregular margin the hypotensity may be accreditable to this complicated distribution of blood vessels in tumors. The base widths of the hypointense areas tended to be broader in patients with subserosal leiomyoma than in those with intramural leiomyoma. Subserosal leiomyomas were compressed directly by the sacral promontory or vertebra, and intramural leiomyomas were compressed indirectly through intervening normal myometrium. The base of the area lay in the myometrium of the uterus in patients with intramural leiomyoma and in tumor tissues in patients with subserosal leiomyoma. In patients with intramural leiomyoma, because blood flow of the myometrium between tumor and the promontory was retained despite compression, the base of the hypointense area in the myometrium tended to be narrow.

The hypointense areas seen in the patients with adenomyosis were nodular in shape, not flare-shaped as in the patients with leiomyoma. An exact reason for the difference in shape is unclear. In

Table. Findings of MR imaging and histopathological studies

Case	Age	Lesion		Hypointense area		Pathology
		Type	Size (mm)	Shape	Size (mm)	
1	30	Intramural leiomyoma	90×60	Flare shape with narrow base	25×20	Cellular leiomyoma
2	48		125×85		50×30	NA
3	32		110×80		20×45	NA
4	53		70×65		15×25	NA
5	27		115×80		40×25	NA
6	38	Subserosal leiomyoma	125×75	Flare shape with broad base	35×15	NA
7	38		91×60		15×10	Leiomyoma with hyalinization
8	31		140×80		55×80	Leiomyoma with hyalinization
9	46		90×75		32×70	Leiomyoma with hyalinization
10	36		85×80		40×30	Usual leiomyoma
11	48	Adenomyosis	120×60	Nodular shape	40×18	Usual adenomyosis
12	53		115×90		25×15	Usual adenomyosis

Note. NA: not available

adenomyosis, involved myometrium might somehow preserve pre-existing original vasculature and have a different pattern of blood supply from that in tumor tissues of leiomyoma. This difference in vascular structure might reflect the difference in the shape of hypointense areas, but further studies are needed.

The area of hypointensity may mimic necrosis or degeneration and thereby confuse the diagnosis and evaluation of a huge uterine mass. Recently, UAE has been performed widely in patients with leiomyomas and adenomyosis who present with menorrhagia. MR imaging is used in the evaluation of the efficacy of UAE. An embolized lesion is depicted as a non-enhanced area on postcontrast T_1-weighted MR images.[11] The hypointense area may mimic embolized tissues and cause overestimation of the effect of UAE.

In conclusion, in the present study, areas of hypointensity may represent functional changes, such as localized decrease in blood flow caused by compression of the sacral promontory. With careful reading of MR images, these areas can be distinguished from true pathological changes, such as degeneration or necrosis. Radiologists should be reminded of this phenomenon to avoid misinterpretation.

References

1. Murase E, Siegelman ES, Outwater EK, Perez-Jaffe LA, Tureck RW. Uterine leiomyomas: histopathologic features, MR imaging findings, differential diagnosis, and treatment. Radiographics 1999; 19:1179–1197.
2. Hricak H, Tscholakoff D, Heinrichs L, et al. Uterine leiomyomas: correlation of MR, histopathologic findings, and symptoms. Radiology 1986; 158: 385–391.
3. Yamashita Y, Torashima M, Takahashi M, et al. Hyperintense uterine leiomyoma at T_2-weighted MR imaging: differentiation with dynamic enhanced MR imaging and clinical implications. Radiology 1993; 189:721–725.
4. Park SW, Kim SH, Cho JY, Yeon KM, Park IA, Park NH. Compression of large uterine myoma by sacral promontory: MR findings. J Comput Assist Tomogr 1998; 22:387–390.
5. Yoshimitsu K, Honda H, Kuroiwa T, et al. Pseudolesions of the liver possibly caused by focal rib compression: analysis based on hemodynamic change. AJR Am J Roentgenol 1999; 172:645–649.
6. Farrer-Brown G, Beilby JO, Tarbit MH. The vascular patterns in myomatous uteri. J Obstet Gynaecol Br Commonw 1970; 77:967–975.
7. Farrer-Brown G, Beilby JO, Rowles PM. Microvasculature of the uterus. An injection method of study. Obstet Gynecol 1970; 35:21–30.
8. Casey R, Rodgers PA, Vollenhoven BJ. An immunohistochemical analysis of fibroid vasculature. Hum Reprod 2000; 15:1469–1475.
9. Siegler AM, Camilien L. Adenomyosis. J Reprod Med. 1994; 39:841–853.
10. Beilby JO, Farrer-Brown G, Tarbit MH. The microvasculature of common uterine abnormalities, other than fibroids. J Obstet Gynaecol Br Commonw 1971; 78:361–368.
11. deSouza NM, Williams AD. Uterine arterial embolization for leiomyomas: perfusion and volume changes at MR imaging and relation to clinical outcome. Radiology 2002; 222:367–374.

JOURNAL OF MAGNETIC RESONANCE IMAGING 26:1133–1138 (2007)

Technical Note

Influence of Inversion Pulse Type in Assessing Lung-Oxygen-Enhancement by Centrically-Reordered Non-Slice-Selective Inversion-Recovery Half-Fourier Single-Shot Turbo Spin-Echo (HASTE) Sequence

Michael Puderbach, MD,[1] Yoshiharu Ohno, MD, PhD,[2*] Hideaki Kawamitsu, BS,[3] Hisanobu Koyama, MD,[2] Daisuke Takenaka, MD,[2] Munenobu Nogami, MD,[2] Makoto Obara, MSc,[4] Marc Van Cauteren, PhD,[4] Hans-Ulrich Kauczor, MD,[1] and Kazuro Sugimura, MD[2]

Purpose: To demonstrate the influence of inversion pulse type and inversion time for assessment of oxygen-enhancement on centrically-reordered non-slice-selective inversion-recovery (IR) half-Fourier single-shot turbo spin-echo (HASTE) sequence.

Material and Methods: Phantoms with and without 100% oxygen and three healthy volunteers were studied with two-dimensional (2D) centrically-reordered non-slice selective IR-HASTE sequence with either composite or block inversion-recovery pulse at increasing inversion times from 200 to 1800 msec. Signal-to-noise ratios (SNRs) of phantom, real signal differences, and relative enhancement ratios of lung parenchyma between oxygen-enhanced and non-oxygen-enhanced MR images on composite and block pulse type were statistically compared at each TI.

Results: SNRs at TIs of 200 and 400 msec using the composite inversion pulse type were significantly lower than those with the block inversion pulse in the in vivo study ($P < 0.05$), although no significant differences were observed in the phantom study and in the in vivo study at inversion times greater than or equal to 600 msec. Real signal intensity (SI) differences at 400 and 600 msec of the composite inversion pulse type were significantly higher than those with the block inversion pulse type ($P < 0.05$). Relative enhancement ratio at 800 msec with the composite inversion pulse were significantly lower than that with the block inversion pulse ($P < 0.05$).

Conclusion: IR pulse type and inversion time have influence on assessment of oxygen-enhancement by centrically-reordered non-slice-selective IR-HASTE sequence.

Key Words: lung; MR; pulse sequence; inversion-recovery; fast imaging
J. Magn. Reson. Imaging 2007;26:1133–1138.

BESIDES HYPERPOLARIZED 3-helium magnetic resonance (MR) imaging (1), oxygen-enhanced MR imaging was initially reported as a potential alternative approach for the visualization of pulmonary ventilation in 1996 (2). Molecular oxygen contains two unpaired electrons and is weakly paramagnetic, and has been suggested for use as a contrast agent for the lungs (2,3).

Recently, several investigators reported that oxygen-enhanced MR imaging is useful for assessment of regional ventilation and oxygen diffusion in animal experimental and human studies (2,4–11). In contrast to standard lung function tests that focus on global pulmonary ventilation, this new MR imaging technique has been suggested to provide unique and important information related to regional ventilation and oxygen diffusion from alveoli to the capillary bed in the lung parenchyma (2,4–11). However, this new technique has some difficulties for the clinical setting due to the inherently low signal intensity (SI) change by oxygen-inhalation and the degradation of image quality due to respiratory and cardiac artifacts. Therefore, different investigators have tried to improve image quality by different means: adapting parallel imaging techniques, gradient-echo sequence or single-shot turbo spin-echo sequence with or without half-Fourier scheme, cardiac- and/or respiratory-triggering technique or breath-holding technique and by changing the phase-encoding scheme from sequentially-reordered to centrically-reordered in the half-Fourier single-shot turbo spin-echo (HASTE) sequence (2,4–13). In addition, a few studies suggested the influence of interecho-spacing or slice-selection of

[1]Department of Radiology, Deutsches Krebsforschungszentrum, Heidelberg, Germany.
[2]Department of Radiology, Kobe University Graduate School of Medicine, Kobe, Japan.
[3]Radiology Devision, Kobe University Hospital, Kobe, Japan.
[4]Philips Medical Systems, Tokyo, Japan.
Contract grant sponsor: Japanese-German Radiological Affiliation.
*Address reprint requests to: Y.O., MD, PhD, Department of Radiology, Kobe University Graduate School of Medicine, 7-5-2 Kusunoki-cho, Chuo-ku, Kobe, Hyogo 650-0017, Japan.
E-mail: yosirad@kobe-u.ac.jp; yosirad@med.kobe-u.ac.jp; yoshiharuohno@aol.com
Received August 10, 2006; Accepted July 3, 2007.
DOI 10.1002/jmri.21105
Published online in Wiley InterScience (www.interscience.wiley.com).

inversion-recovery (IR) pulse for non-oxygen-enhanced and/or oxygen-enhanced MR imaging of the lung (14). These works suggest that we have to consider the influence of various parameters for the clinical setting of oxygen-enhanced MR imaging of the lung.

Although the duration of the composite inversion pulse type is longer, a composite radio frequency (RF) pulse type has been shown to be more tolerant to inhomogeneities of the RF pulse amplitude (B_1) and/or the magnetic field than the block pulse; therefore, it would seem useful to apply this type of pulse prior to the primary excitation pulse to invert the net magnetization (15). Reviewing the literature, some researchers suggested that different inversion pulse types influence or improve the image quality of MR imaging and MR spectroscopy for various nuclear substances in vivo and in vitro studies (15–18). However, so far no one has clearly described the influence of the IR pulse type for the assessment of oxygen-enhancement in the lung by using the IR-HASTE technique. Therefore, we developed a centrically-reordered IR-HASTE sequence with a composite inversion pulse, and implemented the new sequence for oxygen-enhanced MR imaging of the lung.

We hypothesized that the choice of different inversion pulse type on centrically-reordered non-slice-selective IR-HASTE sequence is an important factor for the assessment of regional oxygen-enhancement within the lung at different TI values. The purpose of the present study is to demonstrate the influence of the inversion pulse type and inversion time for the assessment of oxygen-enhancement on centrically-reordered non-slice-selective IR-HASTE sequence.

MATERIALS AND METHODS

Phantom and MR Imaging for Oxygen-Phantom Study

A total of two plastic containers (PR-920L; Takeya Chemical Industry Co., Ltd., Osaka, Japan) filled with 100% pure water were placed into a 1.5-Tesla whole body scanner (Gyroscan Intera T-15; Philips Medical Systems, Best, The Netherlands), in one row simultaneously. The first container contained pure untreated water. The second container contained water that was sputtered by oxygen (15 liters/minute) for five minutes. Then, two-dimensional (2D) dynamic centrically-reordered non-slice-selective IR-HASTE (2D c-IR-HASTE) images with composite ($90°_x$/1.75 msec, $240°_y$/4.67 msec, $90°_x$/1.75 msec) and block (180°/0.5 msec) inversion pulses were obtained at inversion times (TIs) from 200 to 1800 msec in steps of 200 msec by using the body coil. Details of the scan parameters were as follows: TR = 3500 msec, TE = 4 msec, interecho spacing = 4 msec, slice thickness = 10 mm, field of view (FOV) = 400 mm, matrix size = 256 × 256, echo train length = 134, and number of excitations (NEX) = 2. In these sequences, the actual number of phase encoding steps are 134 in this implementation of the single-shot HASTE sequence. A total of 10 dynamic images were obtained in coronal orientation by a single slice through the center of the plastic containers by each sequence.

Volunteers and MR Imaging for Volunteer Study

The institutional review board approved this study, and written informed consent was obtained from all the subjects prior to enrolment in the study. A total of three healthy male volunteers (aged 29, 38, and 41 years; mean 36 years) underwent oxygen-enhanced MR imaging with a respiratory-triggered (expiration) 2D dynamic c-IR-HASTE sequence with non-slice-selective composite ($90°_x$/1.75 msec, $240°_y$/4.67 msec, $90°_x$/1.75 msec) or block (180°/0.5 msec) inversion pulses at different TIs from 200 to 1800 msec in steps of 200 msec in coronal orientation in the same 1.5 T MR unit using the body coil. Details of scan parameters were as follows: TR = 3000–5000 msec, TE = 4 msec, interecho spacing = 4 msec, slice thickness = 10 mm, FOV = 530 mm, matrix size = 256 × 256, echo train length = 134, and NEX = 3. The actual number of phase encoding steps in these sequences was also 134. A total of three NEX were used to reduce pulsation artifacts. The following paradigm for oxygen inhalation was used for each protocol: subjects initially inhaled 21% oxygen (room air) for five dynamic series, then 100% oxygen for five dynamic series (total of 10 dynamic series per TI on each sequence). The administration of 100% oxygen in this manner has been shown to produce oxygen concentrations in the lung of between 60% and 80% (19). The total scan time for each sequence was between 900 msec and 1500 msec per image. The total oxygen-inhalation time per subject was equal to or less than 14 minutes.

Image Analysis

Oxygen-Phantom Study

The images were evaluated using the Program ImageJ version 1.33u (Wayne Rasband, National Institutes of Health [NIH], USA; http://rsb.info.nih.gov/ij). Rectangular regions of interest (ROIs) with an area of 12.4 cm^2 were placed in the center of the both pots and outside the pots for noise evaluation in each image.

On c-IR-HASTE sequences with composite and block inversion pulse types, signal-to-noise ratio (SNR) of oxygen-enhanced and non-oxygen-enhanced MR images at each TI was calculated as follows (20):

$$(SI_{ROI} \div SD_{Back\ ground}) \times (2 - [\pi/2])^{1/2}, \qquad (1)$$

where SI_{ROI} is the SI in the ROI of one of the water-filled container and $SD_{Background}$ is the standard deviation (SD) in the background.

Volunteer Study

For image analysis in the volunteer study, five circular ROIs were used. Four ROIs with an area of 8.9 cm^2 were placed in the upper right, lower right, upper left, and lower left lung field and one ROI with 3.4 cm^2 was placed outside the body. This procedure was performed on all five MR images in each of the nine dynamic sequences using the previously described program (Image J, version 1.33u).

The SNRs of the lung field at each TI of non-oxygen-enhanced and oxygen-enhanced MR images using the

respiratory triggered c-IR-HASTE sequences with each inversion pulse type were calculated using Eq. [1].

To determine the influence of inversion pulse types on direct signal measurement on the subtraction image and/or real T1 changing maps, SI difference between oxygen-enhanced and non-oxygen-enhanced MR images at each TI was calculated with the composite and block inversion pulse types as follows:

$$\Delta SI = SI_{oxygen\text{-}enhanced} - SI_{non\text{-}oxygen\text{-}enhanced}, \quad (2)$$

where $SI_{oxygen\text{-}enhanced}$ and $SI_{non\text{-}oxygen\text{-}enhanced}$ are SIs within the ROI at same dynamic series of oxygen-enhanced and non-oxygen-enhanced MR images.

To determine the influence of the inversion pulse types on the relative enhancement ratio map for assessment of regional oxygen-enhancement, the relative enhancement ratio of lung parenchyma at each TI between oxygen-enhanced and non-oxygen-enhanced MR images by using each sequence type was evaluated using the following formula:

$$\text{Relative enhancement ratio} = |SI_{oxygen\text{-}enhanced} - SI_{non\text{-}oxygen\text{-}enhanced}| \div SI_{non\text{-}oxygen\text{-}enhanced}, \quad (3)$$

where $SI_{oxygen\text{-}enhanced}$ and $SI_{non\text{-}oxygen\text{-}enhanced}$ are SIs within the ROI at same dynamic series of oxygen-enhanced and non-oxygen-enhanced MR images.

Statistical Analysis

Oxygen-Phantom Study

To determine the influence of the inversion pulse type to SNR differences on non-oxygen-enhanced and oxygen-enhanced MR images in the phantom study, SNRs at every TI between the composite and block inversion pulse types were compared by means of Fisher's protected least difference significant test.

Volunteer Study

To determine the influence of the inversion pulse type to SNR differences on non-oxygen-enhanced and oxygen-enhanced MR images in the in vivo study, SNRs at every TI between the composite and block inversion pulse types were compared by means of Fisher's protected least difference significant test.

To assess the influence of the inversion pulse type on the direct SI change and the relative enhancement ratio between non-oxygen-enhanced and oxygen-enhanced MR imaging, real SI differences and relative enhancement ratios of lung parenchyma between oxygen-enhanced and non-oxygen-enhanced MR images at each TI were compared between the composite and block inversion pulse types by using Fisher's protected least difference significant test.

A *P*-value less than 0.05 was considered statistically significant in all statistical analyses.

RESULTS

Oxygen-Phantom Study

SNRs of oxygen-enhanced and non-oxygen-enhanced MR images obtained by c-IR-HASTE sequences with the composite and block inversion pulse types at each TI are shown in Fig. 1. There was no significant difference in SNR at each TI between the composite and block inversion pulse types on oxygen-enhanced and non-oxygen-enhanced MR images ($P > 0.05$).

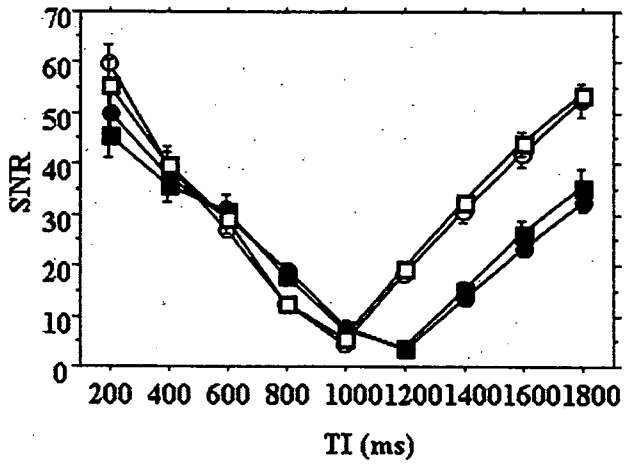

Figure 1. Oxygen phantom: comparison of SNRs of non-oxygen-enhanced MR images between the composite (■) and block (●) inversion pulses at each inversion time (TI) and SNRs of oxygen-enhanced MR images between the composite (□) and block (○) inversion pulses at each TI. There was no significant difference in SNR between the composite and block inversion pulse types on oxygen-enhanced and non-oxygen-enhanced MR images ($P > 0.05$).

Volunteer Study

Representative cases of non-oxygen-enhanced MR images at each TI obtained by the composite and block inversion pulse types are shown in Fig. 2.

Non-oxygen-enhanced and oxygen-enhanced SNRs of the lung parenchyma by using c-IR-HASTE sequences with the composite and block inversion pulse types at each TI are shown in Fig. 3. Non-oxygen-enhanced and oxygen-enhanced SNRs calculated for the ROIs in the lung at 200 and 400 msec of c-IR-HASTE with the composite inversion pulse type were significantly lower than those with the block inversion pulse type (200 msec: $P < 0.0001$, 400 msec: $P < 0.0001$), although there were no significant differences between both inversion pulse types at 600 msec and 1800 msec ($P > 0.05$).

Real SI differences between oxygen-enhanced and non-oxygen-enhanced MR images at each TI on c-IR-HASTE sequences with the composite and block inversion pulse types are shown in Fig. 4. Real SI differences of lung parenchyma at 400 and 600 msec of c-IR-HASTE with the composite inversion pulse type were significantly higher than those with the block inversion pulse type (400 msec: $P < 0.0001$, 600 msec: $P = 0.009$), although there were no significant differences between both inversion pulse types at other TIs ($P > 0.05$).

Relative enhancement ratios at each TI of c-IR-HASTE sequences with the composite and block inversion pulse types at each TI are shown in Fig. 5. Relative

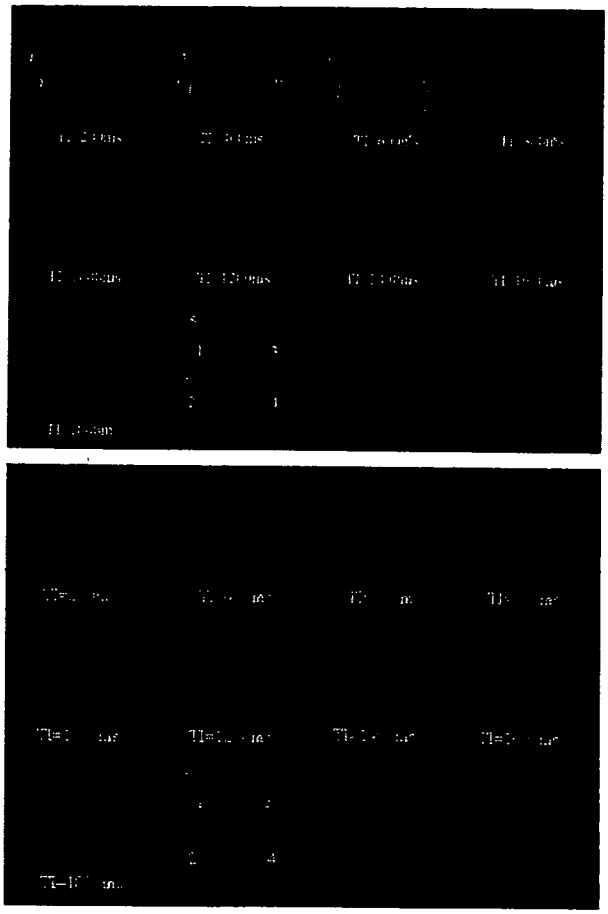

Figure 2. a: Representative case of non-oxygen-enhanced MR images at each TI and ROI placement obtained by c-IR-HASTE with the composite inversion pulse type in a 41-year-old male volunteer. Notice the changing lung parenchyma and vessel signal at each TI. **b:** Representative case of non-oxygen-enhanced MR images at each TI and ROI placement obtained by c-IR-HASTE with the block inversion pulse type in a 41-year-old male volunteer. Notice the changing lung parenchyma and vessel signal at each TI. 1 = right upper lobe, 2 = right lower lobe, 3 = left upper lobe, 4 = left lower lobe, and 5 = ROI outside the volunteer for noise evaluation; ROI size varied between 8.9 cm^2 (lung ROIs) and 3.4 cm^2 (noise ROI).

enhancement ratio of lung parenchyma at 800 msec of c-IR-HASTE with the composite inversion pulse type were significantly lower than that with the block inversion pulse type ($P < 0.0001$), although there were no significant differences between both inversion pulse types at other TIs ($P > 0.05$).

DISCUSSION

Comparing the SNRs of oxygen-enhanced and non-oxygen-enhanced MR images in the phantom study, there were no significant differences between the composite and block inversion pulse types. On IR sequences with the composite and block inversion pulse types a $90°_x/240°_y/90°_x$ RF pulse and a 180° RF pulse are applied prior to the primary excitation pulse to invert the net magnetization. Following this pulse a T1 relaxation occurs in which the net magnetization changes from an inverted condition through zero net magnetization to a relaxed condition. The composite inversion pulse type has been shown to be more tolerant to inhomogeneities of RF pulse amplitude than the block pulse type. Our results demonstrate that the influence of both inversion pulse types on the SNR–inversion time course curves in non-oxygen-enhanced and oxygen-enhanced MR imaging of the phantom study did not result in a significant difference in image quality. This is most likely due to the almost perfect RF and B_0 homogeneity within the phan-

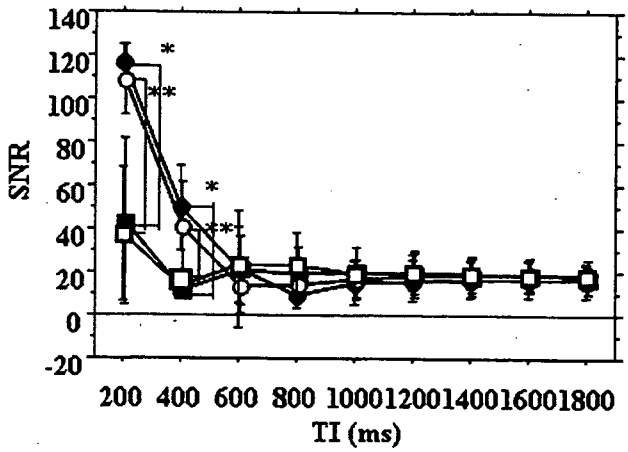

Figure 3. Comparison of SNRs of non-oxygen-enhanced MR images between composite (■) and block (●) inversion pulse at each inversion time (TI) and SNRs of oxygen-enhanced MR images between the composite (□) and block (○) inversion pulse at each TI. On oxygen-enhanced and non-oxygen-enhanced MR images, SNRs of lung at 200 msec and 400 msec on c-IR-HASTE with the composite inversion pulse type were significantly lower than those with the block inversion pulse type (200 msec: $P < 0.0001$, 400 msec: $P < 0.0001$).

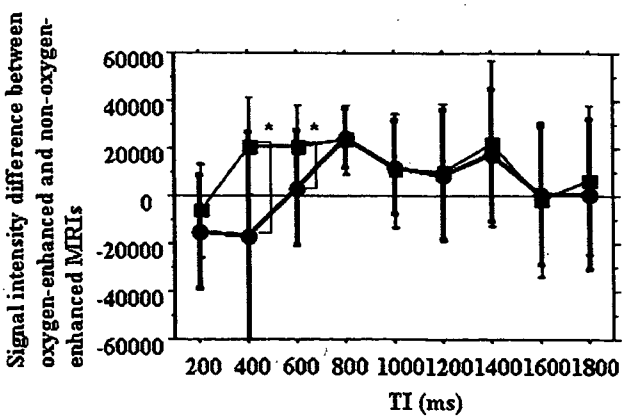

Figure 4. Real SI differences between oxygen-enhanced and non-oxygen-enhanced MR images at each TI on c-IR-HASTE sequences with the composite (■) and block (●) inversion pulse types. Real SI differences of lung parenchyma at 400 msec and 600 msec on c-IR-HASTE with the composite inversion pulse type were significantly higher than those with the block inversion pulse type (400 msec: $P < 0.0001$, 600 msec: $P = 0.009$).

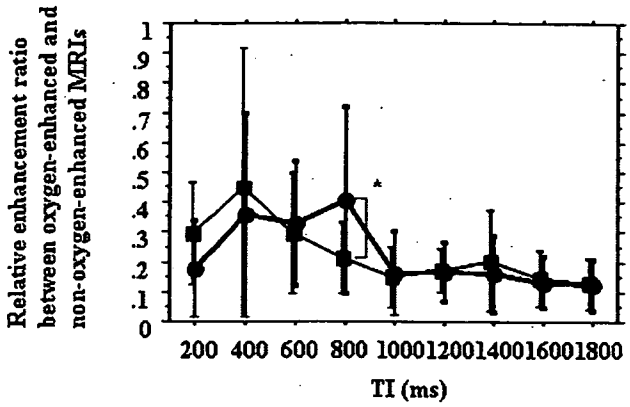

Figure 5. Relative enhancement ratios at each TI of c-IR-HASTE sequences with the composite (■) and block (●) inversion pulse types at each TI. Relative enhancement ratio of lung parenchyma at 800 msec of c-IR-HASTE with the composite inversion pulse type were significantly lower than that with the block inversion pulse type ($P < 0.0001$).

tom, the absence of flow, and the relatively long TI and T2 of the pure water in the phantom.

In the volunteer study, our results showed some differences of the SNR–inversion time curves of both pulse types on non-oxygen-enhanced and oxygen-enhanced MR imaging. On non-oxygen-enhanced and oxygen-enhanced MR imaging, the SNR of the lung at TIs of 200 and 400 msec with the composite pulse were significantly lower than those with the block pulse. In addition, on Figure 2a and b, signal intensities of bone marrow, subcutaneous fat, liver and pulmonary and systemic vasculatures were different. These results suggest that the differences in the SNR between both sequences at 200 and 400 msec are mainly due to differences in the initially inverted magnetization. This difference is caused by a relatively longer duration time and narrow bandwidth of the composite inversion pulse type as compared with the block pulse type. The composite pulse has a bandwidth of 280 Hz. Since the pulse is centered on water, the fat will not be inverted as the difference in frequency between water and fat is larger than 140 Hz. Therefore, spins in bone marrow, subcutaneous fat, and fat in the liver were not inverted, resulting in a constant signal whatever the TI. Further more the pulmonary blood flow, the shorter T2 and the difference in size between the water phantom and the human body are further responsible for this difference.

In contrast to the SNRs of the lung at TIs of 200 and 400 msec with both pulse types, there were no significant differences between both inversion pulse types from 600 msec to 1800 msec on non-oxygen-enhanced and oxygen-enhanced MR imaging. In addition, the SNR of the lung did not recover to its initial level at longer TIs on both sequences on non-oxygen-enhanced and oxygen-enhanced MR imaging. At TIs equal to or longer than the cardiac cycle on both pulse types on non-oxygen-enhanced and oxygen-enhanced MR imaging, the SNRs of the lung on both pulse types are considered to be influenced by the pulmonary blood flow, which removes the inverted protons in the pulmonary blood from the pulmonary circulation to the systemic circulation. In these situations, the SNRs on both pulse type might be caused by the lung parenchyma, which has a significantly lower proton density and shorter T1, T2, and T2* as compared with the pulmonary blood, and may not be able to recover to its initial level. However, further investigation is necessary to completely understand the details of the mechanisms involved. Therefore, we will plan to assess the influence of pulmonary blood flow to SNR in the lung in near future.

Comparing the real SI differences between oxygen-enhanced and non-oxygen-enhanced MR images in the volunteer study, significant differences between the composite and block inversion pulse types and huge SDs were observed at TI = 400 and 600 msec. However, there were no significant differences at TI = 800 msec or more. The ΔSI is positive at TI longer than that of the null point, and ΔSI is negative at TI shorter than that of the null point. These facts suggest that the null point of the block inversion pulse type may be close to 800 msec and the null point of the composite inversion pulse type may be less than 400 msec. These observations are caused by differences in the initially inverted magnetization between the block and composite pulse types. Assessing the direct SI differences on subtracted images as well as on T1-changing maps, the differences of the initially inverted magnetization by each inversion pulse type should be considered for modifying or standardizing the MR sequence for oxygen-enhanced imaging.

On the other hand, comparing the relative enhancement ratio between both pulse types, the relative enhancement ratio of the composite inversion pulse showed no significant difference compared to the block inversion pulse at all TI values except at TI = 800 msec. These results suggest that the assessment of the relative enhancement ratio on oxygen-enhanced MR imaging is less influenced by differences of the initially inverted magnetization.

Our results suggest that TIs except 400 and 600 msec should be adopted for the assessment of the real T1-shortening effect on subtraction images or cross correlation maps, when oxygen-enhanced MR imaging is performed by c-IR-HASTE sequence with the composite inversion pulse type and hope to obtain similar results compared to the block inversion pulse type (2,4,5,11–14,21,22). In addition, our results indicated that TIs except 800 msec should be adopted for evaluation of regional oxygen-enhancement as relative exhancement map, if oxygen-enhanced MR imaging is performed by C-IRHASTE sequence with the composite inversion pulse type and hope to obtain similar results compared to the block inversion pulse type (6-10). Because of the shorter null point, the composite non-slice-inversion pulse allows to shorten the optimal TI for future 3D oxygen-enhanced MR imaging of the entire lung. This saved TI can be used for a prolongation of the data acquisition window during each respiratory cycle, finally resulting in a reduction of scan time. Therefore, the choice of the preparation pulse has huge influence on the image quality of oxygen-enhanced MR imaging, and more attention should be focused on it. Still other

pulse types, most notably adiabatic pulses, and ways of slice-selection need to be evaluated in further studies.

One limitation of the present study is the small number of volunteers included. Furthermore, the MRI system used in this study (Gyroscan Intera T-15; Philips Medical Systems, Best, The Netherlands) did not offer the adiabatic pulse type at the time of the study. Thus only the composite and block inversion pulse types were compared.

In conclusion, the IR pulse type has influence on the assessment of oxygen-enhancement on centrically-reordered non-slice-selective IR-HASTE sequence. The adequate TI for oxygen-enhanced MR imaging should be selected considering the inversion pulse type and the evaluation method for oxygen-enhancement.

REFERENCES

1. van Beek EJ, Wild JM, Kauczor HU, Schreiber W, Mugler JP III, de Lange EE. Functional MRI of the lung using hyperpolarized 3-helium gas. J Magn Reson Imaging 2004;20:540–554.
2. Edelman RR, Hatabu H, Tadamura E, Li W, Prasad PV. Noninvasive assessment of regional ventilation in the human lung using oxygen-enhanced magnetic resonance imaging. Nat Med 1996;2:1236–1239.
3. Young IR, Clarke GJ, Bailes DR, Pennock JM, Doyle FH, Bydder GM. Enhancement of relaxation rate with paramagnetic contrast agents in NMR imaging. J Comput Tomogr 1981;5:543–546.
4. Chen Q, Levin DL, Kim D, et al. Pulmonary disorders: ventilation-perfusion MR imaging with animal models. Radiology 1999;213:871–879.
5. Hatabu H, Tadamura E, Chen Q, et al. Pulmonary ventilation: dynamic MRI with inhalation of molecular oxygen. Eur J Radiol 2001;37:172–178.
6. Loffler R, Muller CJ, Peller M, et al. Optimization and evaluation of the signal intensity change in multisection oxygen-enhanced MR lung imaging. Magn Reson Med 2000;43:860–866.
7. Ohno Y, Chen Q, Hatabu H. Oxygen-enhanced magnetic resonance ventilation imaging of lung. Eur J Radiol 2001;37:164–171.
8. Ohno Y, Hatabu H, Takenaka D, Adachi S, Van Cauteren M, Sugimura K. Oxygen-enhanced MR ventilation imaging of the lung: preliminary clinical experience in 25 subjects. AJR Am J Roentgenol 2001;177:185–194.
9. Muller CJ, Schwaiblmair M, Scheidler J, et al. Pulmonary diffusing capacity: assessment with oxygen-enhanced lung MR imaging preliminary findings. Radiology 2002;222:499–506.
10. Ohno Y, Hatabu H, Takenaka D, Van Cauteren M, Fujii M, Sugimura K. Dynamic oxygen-enhanced MRI reflects diffusing capacity of the lung. Magn Reson Med 2002;47:1139–1144.
11. Ohno Y, Hatabu H, Higashino T, et al. Centrically reordered inversion recovery half-Fourier single-shot turbo spin-echo sequence: improvement of the image quality of oxygen-enhanced MRI. Eur J Radiol 2004;52:200–205.
12. Dietrich O, Losert C, Attenberger U, et al. Fast oxygen-enhanced multislice imaging of the lung using parallel acquisition techniques. Magn Reson Med 2005;53:1317–1325.
13. Jakob PM, Hillenbrand CM, Wang T, Schultz G, Hahn D, Haase A. Rapid quantitative lung (1)H T(1) mapping. J Magn Reson Imaging 2001;14:795–799.
14. Ohno Y, Oshio K, Uematsu H, Nakatsu M, Gefter WB, Hatabu H. Single-shot half-Fourier RARE sequence with ultra-short interecho spacing for lung imaging. J Magn Reson Imaging 2004;20:336–339.
15. Freeman R, Kempsell SP, Levitt MH. Radiofrequency pulse sequences which compensate their own imperfections. J Magn Reson 1980;38:453–479.
16. Xue M, Ng TC, Majors A. Spectral editing of tumor 13C MRS in situ. Magn Reson Med 1990;14:530–537.
17. Dixon WT, Oshinski JN, Trudeau JD, Arnold BC, Pettigrew RI. Myocardial suppression in vivo by spin locking with composite pulses. Magn Reson Med 1996;36:90–94.
18. Hauger O, Dumont E, Chateil JF, Moinard M, Diard F. Water excitation as an alternative to fat saturation in MR imaging: preliminary results in musculoskeletal imaging. Radiology 2002;224:657–663.
19. Bigatello LM. Perioperative respiratory insufficiency. In: Hurford WE, Bailin MT, Davison JK, Hspel KL, Rosow C, editors. Clinical anesthesia procedures of the Massachusetts General Hospital. Philadelphia: Lippincott Williams & Wilkins; 1998. p 618–636.
20. Edelstein WA, Bottomley PA, Pfeifer LM. A signal-to-noise calibration procedure for NMR imaging systems. Med Phys 1984;11:180–185.
21. Mai VM, Chen Q, Bankier AA, Edelman RR. Multiple inversion recovery MR subtraction imaging of human ventilation from inhalation of room air and pure oxygen. Magn Reson Med 2000;43:913–916.
22. Mai VM, Tutton S, Prasad PV, et al. Computing oxygen-enhanced ventilation maps using correlation analysis. Magn Reson Med 2003;49:591–594.